



Article

# Structure and Magnetic Properties of $\text{ErFe}_x\text{Mn}_{12-x}$ ( $7.0 \leq x \leq 9.0$ , $\Delta x = 0.2$ )

Penglin Gao<sup>1,2</sup>, Yuanhua Xia<sup>2</sup>, Jian Gong<sup>2</sup> and Xin Ju<sup>1,\*</sup>

<sup>1</sup> School of Mathematics and Physics, University of Science and Technology Beijing, Beijing 100083, China; gaoyingluo@163.com

<sup>2</sup> Key Laboratory of Neutron Physics and Institute of Nuclear Physics and Chemistry, China Academy of Engineering Physics, Mianyang 621900, China; xiayuanhua2009@126.com (Y.X.); gongjian@hotmail.com (J.G.)

\* Correspondence: jux@ustb.edu.cn

**Abstract:** The magnetic interactions of iron-rich manganese-based  $\text{ThMn}_{12}$  type rare earth metal intermetallic compounds are extremely complex. The antiferromagnetic structure sublattice and the ferromagnetic structure sublattice had coexisted and competed with each other. Previous works are focus on studying magnetic properties of  $\text{RFe}_x\text{Mn}_{12-x}$  ( $x = 0-9.0$ ,  $\Delta x = 0.2$ ). In this work, we obtained a detailed magnetic phase diagram for iron-rich  $\text{ErFe}_x\text{Mn}_{12-x}$  series alloy samples with a fine composition increment ( $\Delta x = 0.2$ ), and studied the exchange bias effect and magnetocaloric effect of samples.  $\text{ErFe}_x\text{Mn}_{12-x}$  series ( $x = 7.0-9.0$ ,  $\Delta x = 0.2$ ) alloy samples were synthesized by arc melting, and the pure  $\text{ThMn}_{12}$ -type phase structure was confirmed by X-ray diffraction (XRD). The neutron diffraction test was used to confirm the Mn atom preferentially occupying the 8i position and to quantify the Mn. The magnetic properties of the materials were characterized by a comprehensive physical property measurement system (PPMS). Accurate magnetic phase diagrams of the samples in the composition range 7.0–9.0 were obtained. Along with temperature decrease, the samples experienced paramagnetic, ferromagnetic changes for samples with  $x < 7.4$  and  $x > 8.4$ , and paramagnetic, antiferromagnetic and ferromagnetic or paramagnetic, ferromagnetic and antiferromagnetic changes for samples with  $7.4 \leq x \leq 8.2$ . The tunable exchange bias effect was observed for sample with  $7.4 \leq x \leq 8.2$ , which resulting from competing magnetic interacting among ferromagnetic and antiferromagnetic sublattices. The maximum magnetic entropy change in an  $\text{ErFe}_{9.0}\text{Mn}_{3.0}$  specimen reached 1.92 J/kg/K around room temperature when the magnetic field change was 5 T. This study increases our understanding of exchange bias effects and allows us to better control them.



**Citation:** Gao, P.; Xia, Y.; Gong, J.; Ju, X. Structure and Magnetic Properties of  $\text{ErFe}_x\text{Mn}_{12-x}$  ( $7.0 \leq x \leq 9.0$ ,  $\Delta x = 0.2$ ). *Nanomaterials* **2022**, *12*, 1586. <https://doi.org/10.3390/nano12091586>

Academic Editor: Jean-Pierre Bucher

Received: 2 April 2022

Accepted: 5 May 2022

Published: 7 May 2022

**Publisher's Note:** MDPI stays neutral with regard to jurisdictional claims in published maps and institutional affiliations.



**Copyright:** © 2022 by the authors. Licensee MDPI, Basel, Switzerland. This article is an open access article distributed under the terms and conditions of the Creative Commons Attribution (CC BY) license (<https://creativecommons.org/licenses/by/4.0/>).

**Keywords:** neutron diffraction; exchange-bias; magnetocaloric effect

## 1. Introduction

Manganese (Mn) is the only 3d-series element that forms a stable  $\text{ThMn}_{12}$ -type structure with rare earth elements [1,2], and it is mainly ferromagnetic and antiferromagnetic [3]. However, the pure  $\text{ThMn}_{12}$ -type rare earth iron compound  $\text{RFe}_{12}$  does not exist. In the early 1980s, Yang et al. [4] found that a stable ternary rare earth iron intermetallic compound  $\text{R}(\text{Fe}_x\text{Mn}_{1-x})_{12}$  could be formed by substitution, thus setting off a surge of research into iron-rich  $\text{ThMn}_{12}$ -type compounds [5]. Subsequent studies have found that a number of tertiary elements can stabilize the  $\text{ThMn}_{12}$  phase; their molecular formulas can be written as  $\text{RFe}_x\text{M}_{12-x}$  or  $\text{R}(\text{Fe}_x\text{M})_{12}$ , where R is a rare earth element and  $\text{M} = \text{Mn}, \text{V}, \text{Cr}, \text{Mo}, \text{W}, \text{Ti}, \text{Si}, \text{Al}, \text{Nb}$  or  $\text{Ga}$  [6–9].

In the  $\text{RMn}_{12}$  alloy, the strong antiferromagnetic interaction between manganese atoms prohibits interaction between rare earth atoms and manganese atoms, so the  $\text{RMn}_{12}$  alloy has two magnetic ordering temperatures: R-R ferromagnetic ordering temperature, and Mn-Mn antiferromagnetic ordering temperature [10]. Iron (Fe) can replace Mn in large

quantities (up to 75%) without changing the crystal structure [11]. Researchers [12–22] have investigated the structure and magnetic transitions of  $R\text{Fe}_x\text{Mn}_{12-x}$ -series materials ( $x = 0\text{--}9.0$ ,  $\Delta x = 1$ ) using neutron diffraction, magnetic measurements and electrical measurements and have found that magnetic interaction in the alloy is extremely complex. As the proportion of Fe increases, the material undergoes an antiferromagnetic  $\rightarrow$  antiferromagnetic + ferromagnetic  $\rightarrow$  ferromagnetic transition. Among the iron-rich  $R\text{Fe}_x\text{Mn}_{12-x}$ -series ( $x = 6.0\text{--}9.0$ ) samples, only materials with integer values of  $x$  have been studied. This composition range includes the magnetic transition stage in which antiferromagnetism and ferromagnetism coexist in the material and plane anisotropy and axis anisotropy compete with each other. Therefore, it is necessary to prepare iron-rich  $R\text{Fe}_x\text{Mn}_{12-x}$ -series ( $x = 6.0\text{--}9.0$ ) alloy samples with a finer composition change to obtain more detailed and complete magnetic phase diagrams, and thus be able to develop new aspects of applications for the material. We first studied  $\text{YFe}_x\text{Mn}_{12-x}$ -series ( $x = 6.0\text{--}9.0$ ) samples to obtain more complete magnetic phase diagrams for the materials and observed very large exchange bias effects and zero field cooling (ZFC) exchange bias effects in the samples [23]. After the discovery of exchange bias effect in Co/CoO nanoparticles, investigations have been mainly focused on a large number of heterogeneous structures such as magnetic bilayers, core-shell nanoparticles, and ferromagnetic nanoparticles embedded in antiferromagnetic matrix compounds [24–26]. So, it is necessary to further study exchange bias for the bulk metallic materials with exchange interactions occurring among the bulk sublattice. Firstly, we study how the magnetic atoms affect the EB effect in  $\text{ThMn}_{12}$ -type compounds. The second-order Stevens factor  $\alpha_J$  for Er atoms is  $>0$ , but the second-order crystal field coefficient (A20) of the rare earth sublattice in the  $\text{ThMn}_{12}$  structure is negative, so magnetocrystalline anisotropy tends to the easy axis. We prepared  $\text{ErFe}_x\text{Mn}_{12-x}$ -series ( $7.0 \leq x \leq 9.0$ ,  $\Delta x = 0.2$ ) alloy specimens have been prepared by arc melting to enable us to investigate the structure and magnetism of the alloy.

## 2. Experimental Methods

$\text{ErFe}_x\text{Mn}_{12-x}$ -series ( $7.0 \leq x \leq 9.0$ ,  $\Delta x = 0.2$ ) alloys were prepared by arc melting. The raw material was melted 4–5 times in an argon gas atmosphere according to the stoichiometric ratio to produce the alloy ingot; 5% more rare earth and 13% more Mn were added to compensate for volatilization in the melting process. A smaller current of 150 A was applied twice for melting, followed by a 200 A current once or twice to control the against excessive Mn volatilization. Specimens from the master alloy ingots were placed in sealed quartz tubes filled with argon and cooled down to room temperature after heat treatment at 1173 K for 2 days.

Phase purity was confirmed by a Cu target X-ray powder diffractometer (PANalytical, Almelo, The Netherlands) at room temperature. The high-resolution neutron diffraction spectrometer ( $\lambda = 0.18846$  nm) of Mianyang Research Reactor (CMRR, Mianyang, China) was used to analyze the crystal structure, in particularly for the positions of Mn atoms. Powdered alloy was bonded into a small cylinder with epoxy resin or the alloy ingot was shattered, so that we could select a small piece of regular shape for magnetic measurement. The ZFC and field cooling (FC) thermomagnetic curves ( $M$ – $T$  curves) of the samples were recorded, and the magnetic hysteresis loops ( $M$ – $H$  loops) of the samples under different FC and temperature conditions were measured by the comprehensive physical property measurement system (PPMS, Quantum Design (San Diego, CA, USA)).

## 3. Experimental Results and Analysis

A phase of the  $\text{ThMn}_{12}$ -type structure was formed in the  $\text{ErFe}_x\text{Mn}_{12-x}$ -series ( $7.0 \leq x \leq 9.0$ ) ingots, and some samples contained a small quantity of the  $\text{Er}(\text{Fe}, \text{Mn})_2$  phase. Heterogeneous  $\text{Er}_2(\text{Fe}, \text{Mn})_{17}$  and  $\text{Er}(\text{Fe}, \text{Mn})_2$  phases are formed in  $\text{ErFe}_x\text{Mn}_{12-x}$ -series ( $7.0 \leq x \leq 9.0$ ) alloys after heat treatment above 1273 K, which differentiates them from  $\text{YFe}_x\text{Mn}_{12-x}$ -series ( $7.0 \leq x \leq 9.0$ ) alloys. Long duration high-temperature heat treatment is therefore not suitable

for this series of materials; 1173 K heat treatment for 48 h will produce homogeneous alloy samples with good crystal shapes.

The X-ray diffraction (XRD) spectra of the samples were examined before and after heat treatment. FullProf software [27] was used to refine the structure of the samples after heat treatment, and the relationship between the lattice constant and the composition of the samples was determined, as shown in Figure 1. With the increasing proportion of Fe, the lattice constant  $a$  decreased linearly and  $c$  remained unchanged.

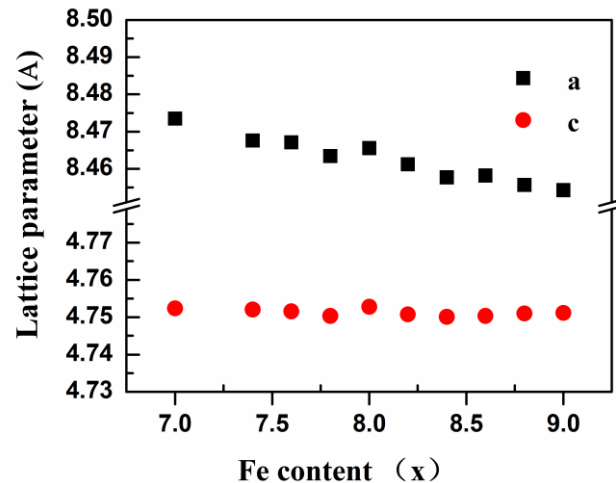


**Figure 1.** Variation of lattice constants  $a$  and  $c$  with Fe content of  $\text{ErFe}_x\text{Mn}_{12-x}$  ( $7.0 \leq x \leq 9.0$ ) series alloys after heat treatment.

The complete neutron diffraction spectra of some heat-treated samples were examined at room temperature, and the structure was refined using FullProf. The fitting spectrum is shown in Figure 2, and the crystal structure parameters are shown in Table 1. The samples formed a pure  $\text{ThMn}_{12}$ -type phase of space group  $I4/mmm$  (139), with rare earth Er atoms occupying the 2a position and Fe and Mn occupying three other unequal positions (8i, 8j, and 8f). Since the coherent neutron scattering lengths of Mn atoms ( $b_{\text{Mn}} = -0.39$ ) and Fe atoms ( $b_{\text{Fe}} = 0.95$ ) are significantly different, the relative proportions of Fe and Mn in the alloy samples can be obtained by fitting neutron diffraction data; the results are shown in Table 1. The Mn atom occupies the 8i position preferentially. The trend of change in the proportion of Mn in the materials was similar to that of the initial materials, although the proportion of Mn was slightly higher, which indicated that the proportion of compensated Mn in the initial materials was relatively high. The lattice constant  $a$  decreased as the proportion of Fe decreased, while the lattice constant  $c$  remained basically unchanged. This is because the Mn atom preferentially occupies the 8i position, and 8i–8i lies in the plane  $ab$ . Changes in the proportion of Mn therefore greatly influences the lattice constants  $a$  and  $b$  but has little effect on the lattice constant  $c$ .

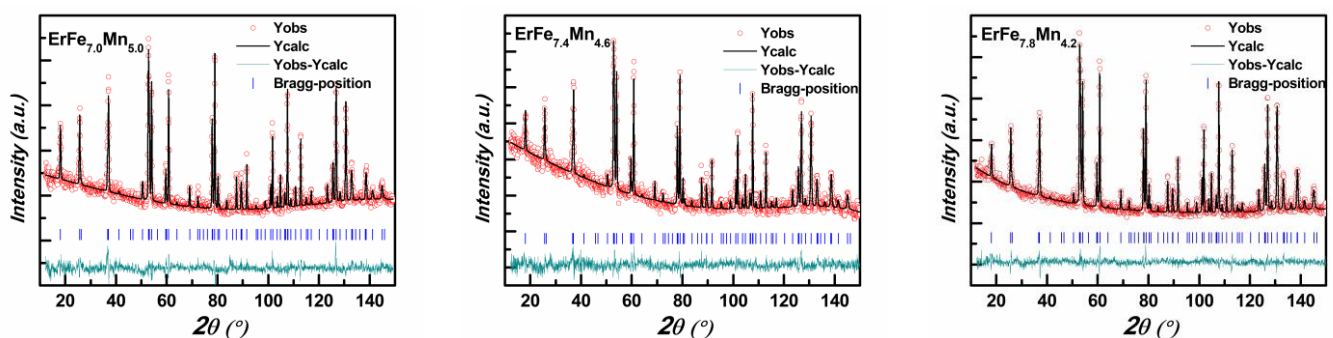


**Figure 2.** Cont.

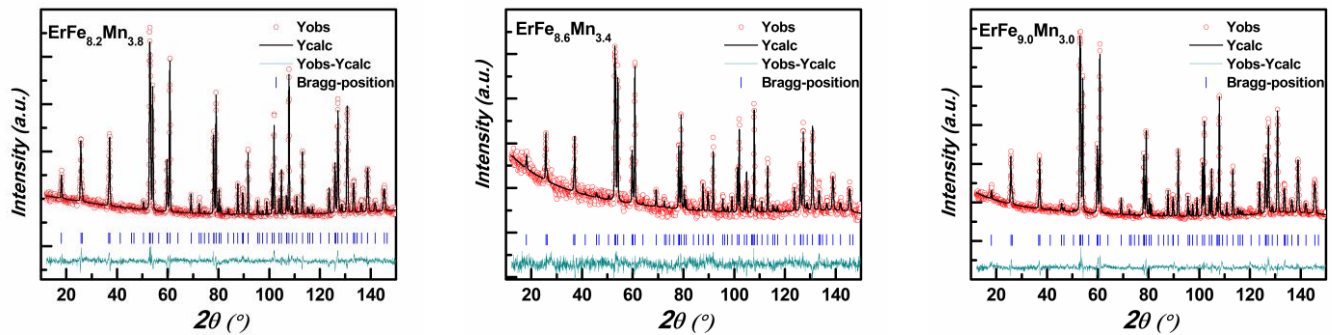


**Figure 2.** Refined neutron diffraction pattern of  $\text{ErFe}_x\text{Mn}_{12-x}$  ( $7.0 \leq x \leq 9.0$ ) series alloys (where red dots are experimental data, black curves are theoretical simulations, blue vertical bars are Bragg diffraction peak positions and the bottom green solid line is the difference curve).

**Table 1.** Information on crystal structure parameters of  $\text{ErFe}_x\text{Mn}_{12-x}$  ( $7.0 \leq x \leq 9.0$ ) series alloys.

$\text{ErFe}_x\text{Mn}_{12-x}$	$a(\text{Å})$	$c(\text{Å})$	occ, Fe, 8i	occ, Fe, 8j	occ, Fe, 8f	$n, \text{Fe}$	$n, \text{Mn}$	$R_{wp}$
$\text{ErFe}_{9.0}\text{Mn}_{3.0}$	8.45469(11)	4.75397(7)	0.476(0)	0.836(4)	0.928(8)	8.96	3.04	5.11
$\text{ErFe}_{8.6}\text{Mn}_{3.4}$	8.45777(24)	4.75346(16)	0.412(4)	0.788(12)	0.892(16)	8.368	3.632	4.54
$\text{ErFe}_{8.2}\text{Mn}_{3.8}$	8.46289(11)	4.75501(7)	0.344(0)	0.792(4)	0.908(8)	8.176	3.824	4.73
$\text{ErFe}_{7.8}\text{Mn}_{4.2}$	8.46758(16)	4.75572(11)	0.300(0)	0.704(8)	0.832(8)	7.344	4.656	3.88
$\text{ErFe}_{7.4}\text{Mn}_{4.6}$	8.47191(24)	4.75547(16)	0.284(0)	0.640(8)	0.764(8)	6.752	5.248	3.29
$\text{ErFe}_{7.0}\text{Mn}_{5.0}$	8.47767(19)	4.75605(13)	0.232(0)	0.636(4)	0.796(8)	6.656	5.344	7.28

Figure 3 shows the thermomagnetic curves of  $\text{ErFe}_x\text{Mn}_{12-x}$ -series ( $7.0 \leq x \leq 9.0$ ) alloy samples in an external magnetic field of 50 Oe.  $T_C$  represents the Curie temperature,  $T_N$  is the Néel temperature,  $T_C$  and  $T_N$  is obtained by differentiating the  $M-T$  curves under FC.  $T_f$  is the temperature corresponding to the bifurcation point in the ZFC and FC magnetization curves. As can be seen from the figure, the ZFC and FC  $M-T$  curves of the samples both clearly bifurcated as the temperature decreased.  $T_f$  was slightly lower than the paramagnetic–ferromagnetic transition temperature of the samples due to the coexistence of Er–Er and Fe–Fe ferromagnetic exchanges interactions. Er–Fe, Er–Mn, Fe–Mn and Mn–Mn antiferromagnetic exchanges interactions, all interactions compete with each other, leading to spin frustration in the samples at low temperatures. For samples with  $x > 7.2$ , the FC  $M-T$  curves initially increased to the maximum value and then decreased gradually as the temperature decreased. The curve steepened, and both the speed and amplitude of bending increased as the proportion of Fe decreased; it reached the maximum for  $x = 7.8$  and then began to decrease and disappeared for  $x = 7.2$ . The magnetization curves for  $x > 7.2$  samples were typical of ferrimagnetism magnetization curves. This was because light rare earth lattices and metal lattices are ferromagnetically arranged and heavy rare earth lattices and metal lattices are antiferromagnetically arranged in rare earth intermetallic compounds with a  $\text{ThMn}_{12}$ -type structure. Er is a heavy rare earth atom, so the samples had a ferrimagnetic structure in which the lattice magnetic moments of rare earth and transition metals were inversely arranged. As the temperature decreased, the magnetic moments of rare earth in the lattice increased rapidly and magnetic moments of transition metals increased slowly; the total magnetic moments of the samples initially increased to the maximum value and then decreased rapidly, and even showed a negative magnetic susceptibility. The  $x = 7.2$  and  $x = 7.0$  samples behave like pure ferro- or ferrimagnetic samples where high coercivity has developed already close to  $T_C$ . This causes the maximum in the ZFC curves very close to  $T_C$ .

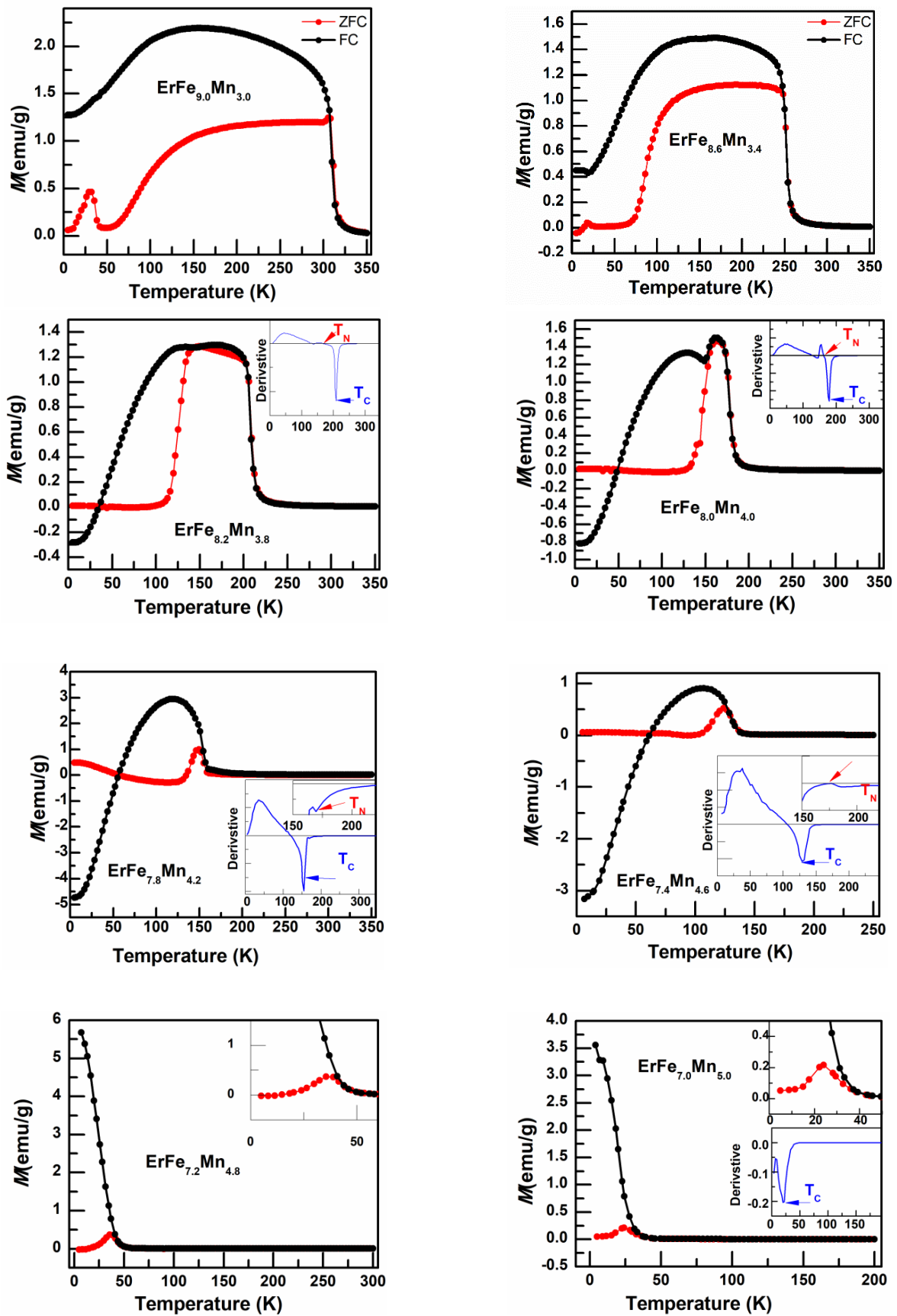


Figure 3.  $M$ – $T$  curves for  $\text{ErFe}_x\text{Mn}_{12-x}$  ( $7.0 \leq x \leq 9.0$ ) series alloys under zero field cooling (ZFC) and field cooling (FC) conditions,  $H = 50$  Oe. (The inset shows the  $M$ – $T$  curves under FC after differentiation.)

In the  $\text{YFe}_x\text{Mn}_{12-x}$ -series ( $6.0 \leq x \leq 8.8$ ) samples, as the proportion of Fe decreased, the  $T_C$  of the alloy rapidly decreased and the  $T_N$  slowly increased; the antiferromagnetic exchange magnetic ordering temperature of Mn-Mn was observed [23]. After rare earth Er atoms with magnetic moments replaced Y atoms without magnetic moments, the antiferromagnetic order of Mn-Mn was suppressed; the obvious antiferromagnetic order of Mn-Mn was only observed in the samples with the Fe proportion  $7.4 \leq x \leq 8.2$ . The magnetic ordering temperature is shown in Table 2. Similar to  $\text{YFe}_x\text{Mn}_{12-x}$ , the ferromagnetic transition temperature of the alloy materials decreased rapidly as the proportion of Fe decreased.

**Table 2.** Magnetic ordering temperature, exchange bias field and coercive force field of  $\text{ErFe}_x\text{Mn}_{12-x}$  ( $7.0 \leq x \leq 9.0$ ) series alloys.

$\text{ErFe}_x\text{Mn}_{12-x}$	$T_C$ (K)	$T_f$ (K)	$T_N$ (K)	$H_E$ (kOe)	$H_C$ (kOe)
	50 Oe	50 Oe	50 Oe	1000 Oe	1000 Oe
$\text{ErFe}_{9.0}\text{Mn}_{3.0}$	310	306			
$\text{ErFe}_{8.6}\text{Mn}_{3.4}$	250	248		−0.22	1.28
$\text{ErFe}_{8.2}\text{Mn}_{3.8}$	208	203	142	11.73	2.97
$\text{ErFe}_{8.0}\text{Mn}_{4.0}$	178	170	163		
$\text{ErFe}_{7.8}\text{Mn}_{4.2}$	154	160	169	6.615	9.54
$\text{ErFe}_{7.4}\text{Mn}_{4.6}$	128	126	176	11.08	4.52
$\text{ErFe}_{7.2}\text{Mn}_{4.8}$	22	44			
$\text{ErFe}_{7.0}\text{Mn}_{5.0}$	22	36		−1.27	28.11

Figure 4 shows the magnetic phase diagram of the  $\text{ErFe}_x\text{Mn}_{12-x}$ -series ( $7.0 \leq x \leq 9.0$ ) alloys. The samples with  $x < 7.4$  or  $x > 8.4$  were mainly ferromagnetic. The samples with  $7.4 \leq x \leq 8.2$  were ferromagnetic and antiferromagnetic, and only the samples in this range of composition showed antiferromagnetic orders between different transition metal lattices.  $\text{YFe}_x\text{Mn}_{12-x}$ -series samples showed a clear exchange bias effect in the region where ferromagnetic interaction and antiferromagnetic interaction compete most intensely [23].  $\text{ErFe}_x\text{Mn}_{12-x}$ -series samples may therefore similarly display exchange bias effects for  $7.4 \leq x \leq 8.2$ . The FC  $M-H$  loops of some samples were measured, and the results are shown in Figure 5. The FC  $M-H$  loops of  $\text{ErFe}_{8.2}\text{Mn}_{3.8}$ ,  $\text{ErFe}_{7.8}\text{Mn}_{4.2}$  and  $\text{ErFe}_{7.4}\text{Mn}_{4.6}$  samples all clearly had lateral shifts. The  $x = 7.4$  and  $x = 7.8$  samples had high coercivity, and the  $M-H$  loops were not completely closed when the applied field was 5T. The  $M-H$  loops were asymmetric, and lateral and vertical shifts occurred simultaneously. This indicates that the samples had very strong magnetocrystalline anisotropy at low temperatures, and that the antiferromagnetic interaction between the rare earth lattice and the transition metal lattice was the source of the anisotropy. When combined with the  $\text{YFe}_x\text{Mn}_{12-x}$ -series experimental results, we see that the exchange bias effect can be controlled by doping different rare earth elements in addition to altering the ratios of Fe and Mn.

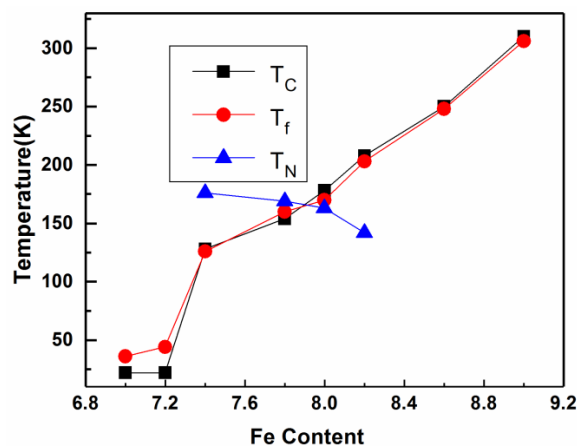


**Figure 4.** The magnetic phase diagram of  $\text{ErFe}_x\text{Mn}_{12-x}$  ( $7.0 \leq x \leq 9.0$ ) series alloys.

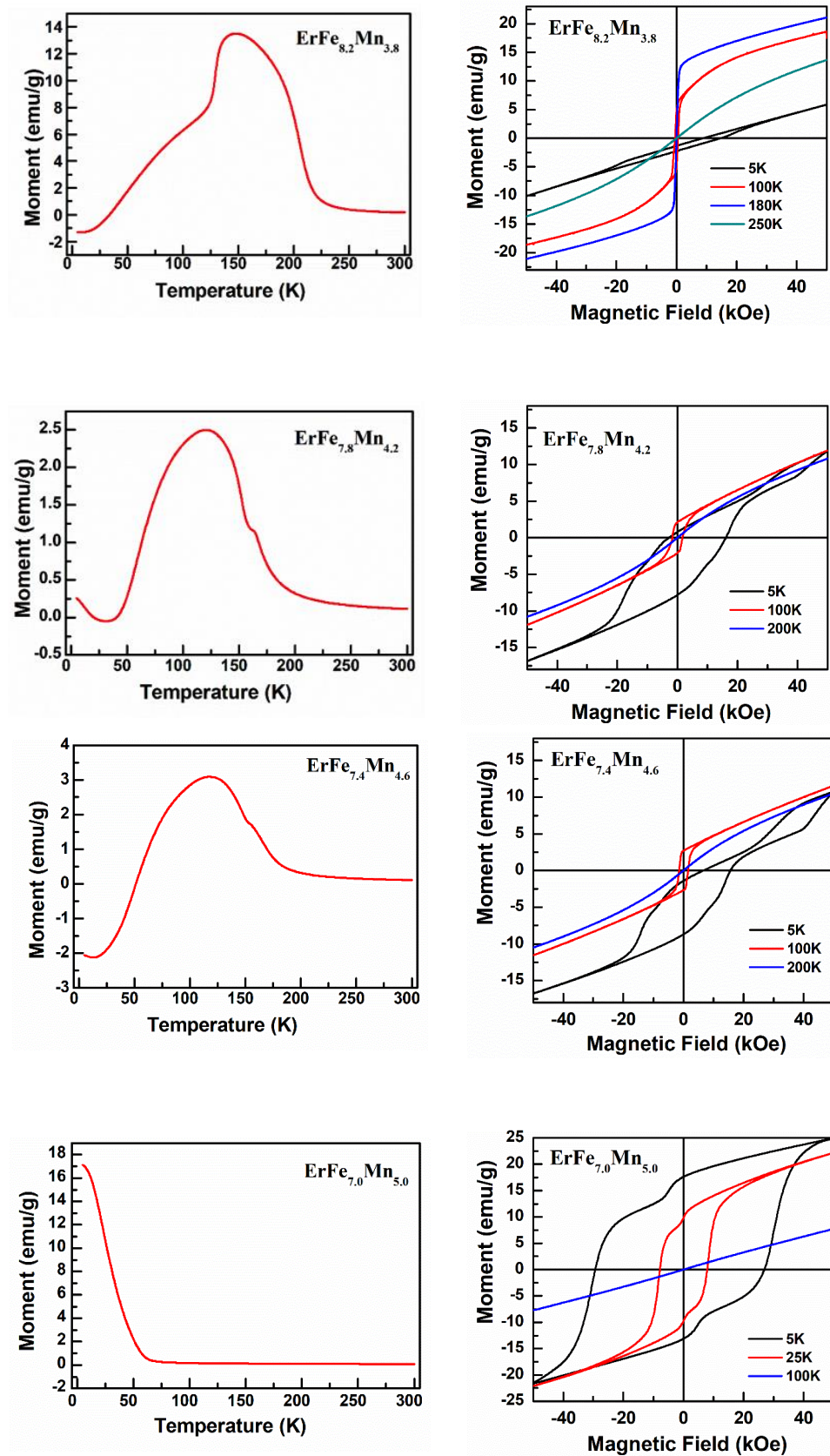


**Figure 5.**  $M-T$  curve under field cooling condition ( $H = 1000$  Oe) and  $M-H$  curve after 1000 Oe field cooling of  $\text{ErFe}_x\text{Mn}_{12-x}$  ( $7.0 \leq x \leq 9.0$ ) series alloys.

The  $\text{ErFe}_{9.0}\text{Mn}_{3.0}$  compound had a Curie temperature of 310 K, and which is near the room temperature. The reverse magnetic moment of Er atom is decrease drastically as temperature increasing, so the samples may have had a considerable magnetocaloric effect near the Curie temperature. The isothermal magnetization curves in the temperature range 270–340 K were created, and are shown in Figure 6. The figure shows that as the temperature increased, magnetization intensity gradually decreased, and ferromagnetism was gradually transformed into paramagnetism. The isothermal magnetization curves were transformed to obtain the Arrott plot, as shown in Figure 7, in order to determine the type of phase transition occurring. There was no S-shaped curve in the Arrott plot, and no negative curve slope was observed, so the phase transition of the materials was also a second-order phase transition.

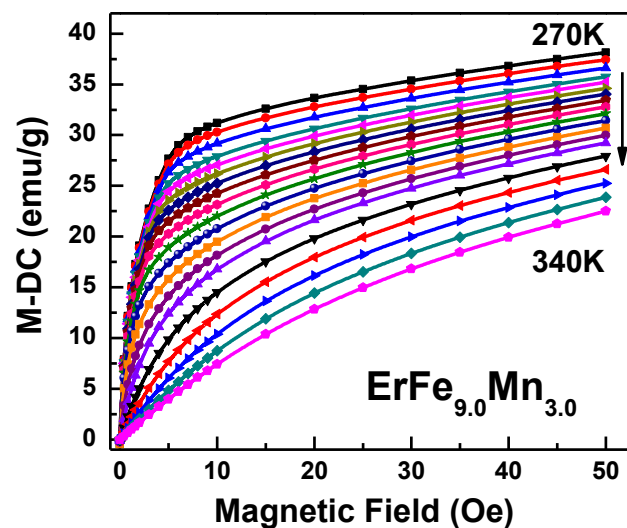


Figure 6. Isothermal magnetization curve of  $\text{ErFe}_{9.0}\text{Mn}_{3.0}$ .

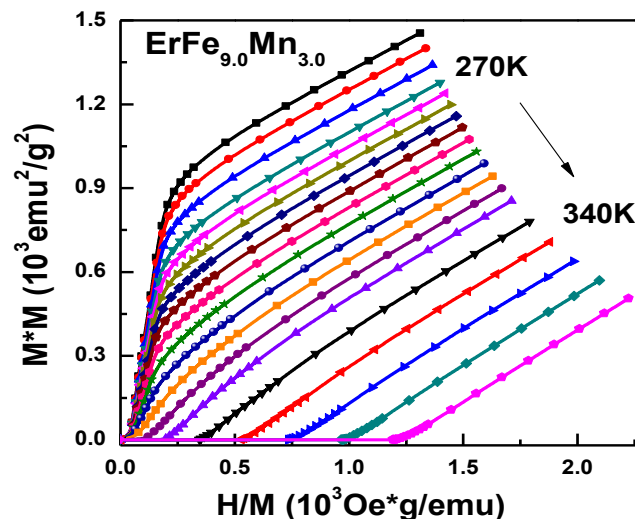


Figure 7. Arrott curve of  $\text{ErFe}_{9.0}\text{Mn}_{3.0}$ .

The Maxwell relation was used to calculate the isothermal magnetic entropy change in the samples from the isothermal magnetization curves at different temperatures, as shown in Figure 8. The calculated maximum value of the magnetic entropy changes when an applied field change of 50 kOe reaches 1.92 J/kg/K. The peak of  $-\Delta S_M$  at 312.5 K corresponds to the ferromagnetic to paramagnetic phase transition, because the magnetization changes drastically near the Curie temperature. Although the maximum  $-\Delta S_M$  of  $\text{ErFe}_{9.0}\text{Mn}_{3.0}$  is not as large as that of some other magnetic refrigerant materials [28], the  $|\Delta S_M|$  vs.

$T$  curve of  $\text{ErFe}_{9.0}\text{Mn}_{3.0}$  is significantly broader compared with other materials, which is favorable for active magnetic refrigeration. Additionally, the magnetocaloric effect was caused by the second-order phase transition near the Curie temperature, and the thermal hysteresis and magnetic hysteresis during phase transition were both very small, which has benefits in the practical application of the material.

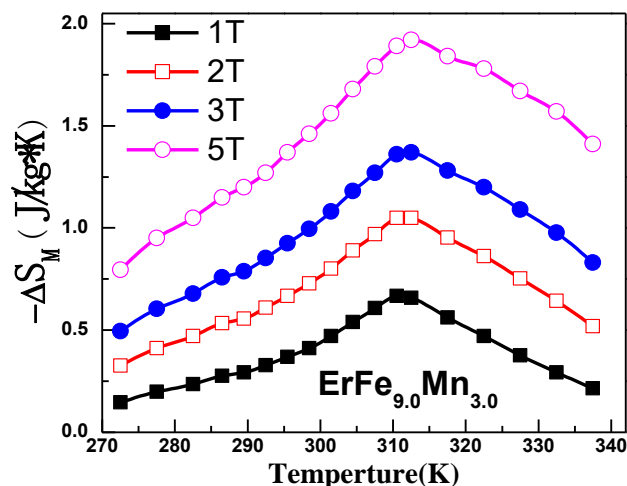


Figure 8. Isothermal magnetic entropy change with temperature for  $\text{ErFe}_{9.0}\text{Mn}_{3.0}$ .

#### 4. Conclusions

$\text{ThMn}_{12}$ -type single phase samples with different Fe/Mn ratios were prepared by arc melting and heat treatment, and the magnetic phase diagrams of  $\text{ErFe}_x\text{Mn}_{12-x}$ -series ( $7.0 \leq x \leq 9.0$ ) samples were obtained by magnetic measurement. At low temperatures, samples with  $x < 7.4$  and  $x > 8.4$  exhibited ferromagnetism, and ferromagnetism and antiferromagnetism coexisted in samples with  $7.4 \leq x \leq 8.2$ , with an FC exchange bias effect. The magnetic interaction between transition metal lattices in  $\text{ThMn}_{12}$ -type structural materials can be changed by substituting non-magnetic Y atoms with rare earth Er atoms with magnetic moments. In this study, Y atoms were completely replaced; in the following study, we will partially replace them to finely modulate the exchange bias effect and the magnetocaloric effect of the materials.

**Author Contributions:** Conceptualization, P.G. and Y.X.; methodology, P.G. and Y.X.; validation, P.G. and Y.X.; formal analysis, P.G. and Y.X.; investigation, P.G. and Y.X.; resources, P.G. and Y.X.; data curation, P.G. and Y.X.; writing—original draft preparation, P.G. and Y.X.; writing—review and editing, P.G. and Y.X.; visualization, P.G. and Y.X.; supervision, J.G. and X.J.; funding acquisition, J.G. and X.J. All authors have read and agreed to the published version of the manuscript.

**Funding:** This research was funded by the National Natural Science Foundation of China, grant number 11504348.

**Data Availability Statement:** The data presented in this study are available in this article.

**Conflicts of Interest:** The authors declare no conflict of interest.

#### References

1. Florio, J.V.; Rundle, R.E.; Snow, A.I. Compounds of Thorium with Transition Metals. I. The Thorium-Manganese System. *Acta Cryst.* **1952**, *5*, 449. [CrossRef]
2. Deportes, J.; Givord, D.; Lemaire, R.; Nagai, H. Magnetic interactions in the R-Mn<sub>12</sub> compounds. *Physica B+C* **1977**, *86–88*, 69–70. [CrossRef]
3. Kirchmayr, H.R. Magnetic properties of rare earth—Manganese compounds. *IEEE Trans. Magn.* **1966**, *2*, 493–499. [CrossRef]
4. Yang, Y.C. Structural and magnetic properties of  $\text{Y}(\text{Mn}(1-x)\text{Fe}_x)_{12}$ . *Acta Metall. Sin.* **1981**, *17*, 355–358.
5. Li, H.S.; Coey, J.M.D. *Handbook of Magnetic Materials*; Bushcaw, K.H.J., Ed.; Elsevier Science Publishers B.V.: Amsterdam, The Netherlands, 1991; Volume 6, pp. 6–41.
6. Mooij, D.B.; De Buschow, K.H.J. Some novel ternary  $\text{ThMn}_{12}$ -type compounds. *J. Less Common Met.* **1988**, *136*, 207–215. [CrossRef]

7. Ohashi, K.; Tawara, Y.; Osugi, R.; Tawara, Y. The magnetic and structural properties of R-Ti-Fe ternary compounds. *IEEE Trans. Magn.* **1987**, *23*, 3101–3103. [[CrossRef](#)]
8. Wang, X.Z.; Chevalier, B.; Berlureau, T.; Etourneau, J.; Coey, J.M.D.; Cadogan, J.M. Iron-rich pseudobinary alloys with the ThMn12 structure obtained by melt spinning: Gd(FenAl12–n), n = 6, 8. *J. Less Common Met.* **1988**, *138*, 235–240. [[CrossRef](#)]
9. Muller, K.H. Magnetic material R, Fe, Mo, (Co) with ThMn12 structure. *J. Appl. Phys.* **1988**, *64*, 249–251. [[CrossRef](#)]
10. Okamoto, N.; Nagai, H.; Yoshie, H.; Tsujimura, A.; Hihara, T. The coexistence of ferromagnetic and antiferromagnetic interactions in the GdMn12 compound. *J. Magn. Magn. Mater.* **1987**, *70*, 299–300. [[CrossRef](#)]
11. Yang, Y.C.; Kebe, B.; James, W.J.; Deportes, J.; Yelon, W. Structural and magnetic properties of Y(Mn1–xFex)12. *J. Appl. Phys.* **1981**, *52*, 2077–2078. [[CrossRef](#)]
12. Amako, Y.; Saoka, S.; Yoshie, H.; Nagai, H.; Adachi, K. Antiferromagnetic Ordering Temperature of RMn12–xFex (R = Rare Earth). *J. Phys. Soc. Jpn.* **1995**, *64*, 1860–1861. [[CrossRef](#)]
13. Stankiewicz, J.; Bartolome, J.; Morales, M.; Bacmann, M.; Fruchart, D. Resistivity of RMn12–xFex alloys. *J. Appl. Phys.* **2001**, *90*, 5632–5636. [[CrossRef](#)]
14. Morales, M.; Bacmann, M.; Wolfers, P.; Fruchart, D.; Ouladdiaf, B. Magnetic properties and interactions in the RMn12–xFex series R(Y, Ho, Er, Nd; x ≤ 9). *Phys. Rev. B* **2001**, *64*, 144426. [[CrossRef](#)]
15. Mao, W.H.; Yang, J.B.; Cheng, B.P.; Yang, Y.C. Unusual magnetic properties of Ho(Fe0.6Mn0.4)12. *Solid State Commun.* **1999**, *109*, 655–659. [[CrossRef](#)]
16. Dong, S.Z.; Yang, J.; Yang, Y.C. Structure and Magnetic Properties of Y(Fe1–xMnx)12 Compounds and Their Nitrides (x = 0.2 and 0.4). *Solid State Commun.* **1995**, *94*, 809–812. [[CrossRef](#)]
17. Stankiewicz, J.; Bartolome, J.; Fruchart, D. Spin Disorder Scattering in Magnetic Metallic Alloys. *Phys. Rev. Lett.* **2002**, *89*, 106602. [[CrossRef](#)] [[PubMed](#)]
18. Yang, J.B.; Yelon, W.B.; James, W.J.; Cai, Q.S.; Eckert, D.; Handstein, A.; Muller, K.H.; Yang, Y.C. Structural and magnetic properties of RFexMn12–x, (R = Ho, Y). *Phys. Rev. B* **2002**, *65*, 064444. [[CrossRef](#)]
19. Stankiewicz, J.; Bartolome, J. Magnetic scattering in RMn12–xFex alloys. *Phys. Rev. B* **2002**, *67*, 092409. [[CrossRef](#)]
20. Pique, C.; Abad, E.; Blanco, J.A.; Burriel, R.; Fernandez-Diaz, M.T. Interplay between competing exchange interactions and magnetocrystalline anisotropies in YFexMn12–x: The magnetic phase diagram. *Phys. Rev. B* **2005**, *71*, 174422. [[CrossRef](#)]
21. Shelyapina, M.G.; Morales, M.; Bacmann, M.; Baudalet, F.; Fruchart, D.; Giorgetti, C.; Hlil, E.K.; Krill, G.; Wolfers, P. Magnetic properties of RMn12–xFex type compounds: I. X-ray magnetic circular dichroism study of the ErMn12–xFex series with x = 0, 7, 8 and 9. *J. Alloys Compd.* **2004**, *368*, 84–93. [[CrossRef](#)]
22. Pique, C.; Blanco, J.A.; Burriel, R.; Abad, E.; Artigas, M.; Fernandez-Diaz, M.T. Influence of 3d-4f interactions in the magnetic phases of RFexMn12–x (R = Gd, Tb, and Dy) compounds: Coexistence of ferromagnetism and antiferromagnetism at different crystallographic sites. *Phys. Rev. B* **2007**, *75*, 224424. [[CrossRef](#)]
23. Xia, Y.H.; Wu, R.; Zhang, Y.F.; Liu, S.Q.; Du, H.L.; Han, J.Z.; Wang, C.S.; Chen, X.P.; Xie, L.; Yang, Y.C.; et al. Tunable giant exchange bias in the single-phase rare-earth–transition-metal intermetallics YMn12–xFex with highly homogenous intersublattice exchange coupling. *Phys. Rev. B* **2017**, *96*, 064440. [[CrossRef](#)]
24. Nogués, J.; Schuller, I.K. Exchange bias. *J. Magn. Magn. Mater.* **1999**, *192*, 203–232. [[CrossRef](#)]
25. Nogués, J.; Sort, J.; Langlais, V.; Skumryev, S.; Suriñach, S.; Muñoz, J.S.; Baró, M.D. Exchange bias in nanostructures. *Phys. Rep.* **2005**, *422*, 65–117. [[CrossRef](#)]
26. Giri, S.; Patra, M.; Majumdar, S. Exchange bias effect in alloys and compounds. *J. Phys. Condens. Matter* **2011**, *23*, 073201. [[CrossRef](#)] [[PubMed](#)]
27. Rodríguez-Carvajal, J. Recent advances in magnetic structure determination by neutron powder diffraction. *Physica B* **1993**, *192*, 55–69. [[CrossRef](#)]
28. Zarkevich, N.A.; Zverev, V.I. Viable Materials with a Giant Magnetocaloric Effect. *Crystals* **2020**, *10*, 815. [[CrossRef](#)]